Tunnelling and Underground Space Technology 98 (2020) 103336

Contents lists available at ScienceDirect

Tunnelling and Underground Space Technology

journal homepage: www.elsevier.com/locate/tust

Influence of spatially varying thickness on load-bearing capacity of shotcrete

William Bjureland*, Fredrik Johansson, Johan Spross, Stefan Larsson

Department of Civil and Architectural Engineering, KTH Royal Institute of Technology, SE-100 44 Stockholm, Sweden

ARTICLE INFO

Keywords:
Rock engineering
Tunnel
Shotcrete
Reliability-based methods

ABSTRACT

A common approach to verify a shotcrete layer's ability to secure blocks that can exist between rockbolts in a tunnel is to use analytical calculations. For this situation, an attractive approach to account for variability in the shotcrete parameters is to use reliability-based methods. Variability can then be accounted for by assigning suitable probability distributions to all relevant input parameters. Structural safety can be ensured by verifying that the probability of limit exceedance is smaller than an acceptable target probability of failure. However, even though analytical calculations and reliability-based methods can be used to design shotcrete support, one of the commonly made basic assumptions is that the load-bearing capacity of the shotcrete is governed by the spatial average of the input parameters. Thus, the spatial variability of the parameters are neglected. As a result, if the capacity is governed by the lowest value of a certain parameter, this assumption is non-conservative. In this paper, we present a novel approach in which the minimum of either the spatial average of a shotcrete slab of varying thickness, or the spatial average along the periphery of a loose block of that same slab, is used to estimate the load-bearing capacity of the shotcrete in a tunnel. The approach is based on results from numerical simulations of a shotcrete slab that we perform to investigate the effect that a spatially varying thickness has on the flexural load-bearing capacity of the slab. The results from the simulations show that the shotcrete's flexural load-bearing capacity might be overestimated when using the spatial average of shotcrete thickness between four rockbolts in design. Using the presented approach, the spatial variability of shotcrete thickness can be accounted for in practical design of tunnels without complex and time-consuming numerical simulations.

1. Introduction

To verify a shotcrete layer's ability to secure blocks that can exist between rockbolts in a tunnel, a common approach is to use analytical calculations (e.g. Holmgren, 1979, 1987, 1992; Barrett and McCreath, 1995; Nilsson, 2003; Banton et al., 2004; Lindfors et al., 2015; Bjureland et al., 2019). The shotcrete support is then idealized into a conditional correlated structural system which is governed by three main failure modes: direct shear, punching shear, or flexural failure (Fig. 1), all of which are correlated to and conditional upon the existence of sufficient adhesion in the rock–shotcrete interface along the circumference of the loose block (Barrett and McCreath, 1995; Bjureland et al., 2019). In essence, if the adhesion is sufficient, the load-bearing capacity of the shotcrete is governed by its ability to withstand the load from the loose block through its direct shear capacity along the circumference of the block; if the adhesion is insufficient, the shotcrete's load-bearing capacity is instead governed by its ability to withstand the punching shear of the systematically installed rockbolts or by its ability to withstand bending moments arising from the load of the loose block, i.e. its flexural capacity.

To account for variability in the shotcrete parameters incorporated in the analytical calculations, an attractive approach, which is accepted in the Eurocodes (CEN, 2002), is to use reliability-based methods. Such methods have previously been applied to a number of rock engineering problems (e.g. Celestino et al., 2006; Jimenez-Rodriguez et al., 2006; Jimenez-Rodriguez and Sitar, 2007; Bagheri, 2011; Langford, 2013; Low and Einstein, 2013; Lü et al., 2013; Bjureland et al., 2017; Matarawi and Harrison, 2017; Napa-García et al., 2017; Bjureland et al., 2019). In these methods, variability is accounted for by assigning suitable statistical distributions to all relevant input parameters; in the design of shotcrete, statistical distributions such as those suggested by Bernard and Xu (2017), Bernard and Xu (2019), and Bjureland et al. (2019) can be used. Structural safety is ensured by verifying that the probability of limit exceedance is smaller than an acceptable target probability of failure.

However, even though analytical calculations and reliability-based methods can be used to design shotcrete support against loose blocks in a tunnel, as discussed in Bjureland et al. (2019), the common

* Corresponding author.
E-mail addresses: william.bjureland@byv.kth.se (W. Bjureland), fredrik.johansson@byv.kth.se (F. Johansson), johan.spross@byv.kth.se (J. Spross), stefan.larsson@byv.kth.se (S. Larsson).

https://doi.org/10.1016/j.tust.2020.103336
Received 18 July 2019; Received in revised form 19 December 2019; Accepted 3 February 2020
Available online 12 February 2020

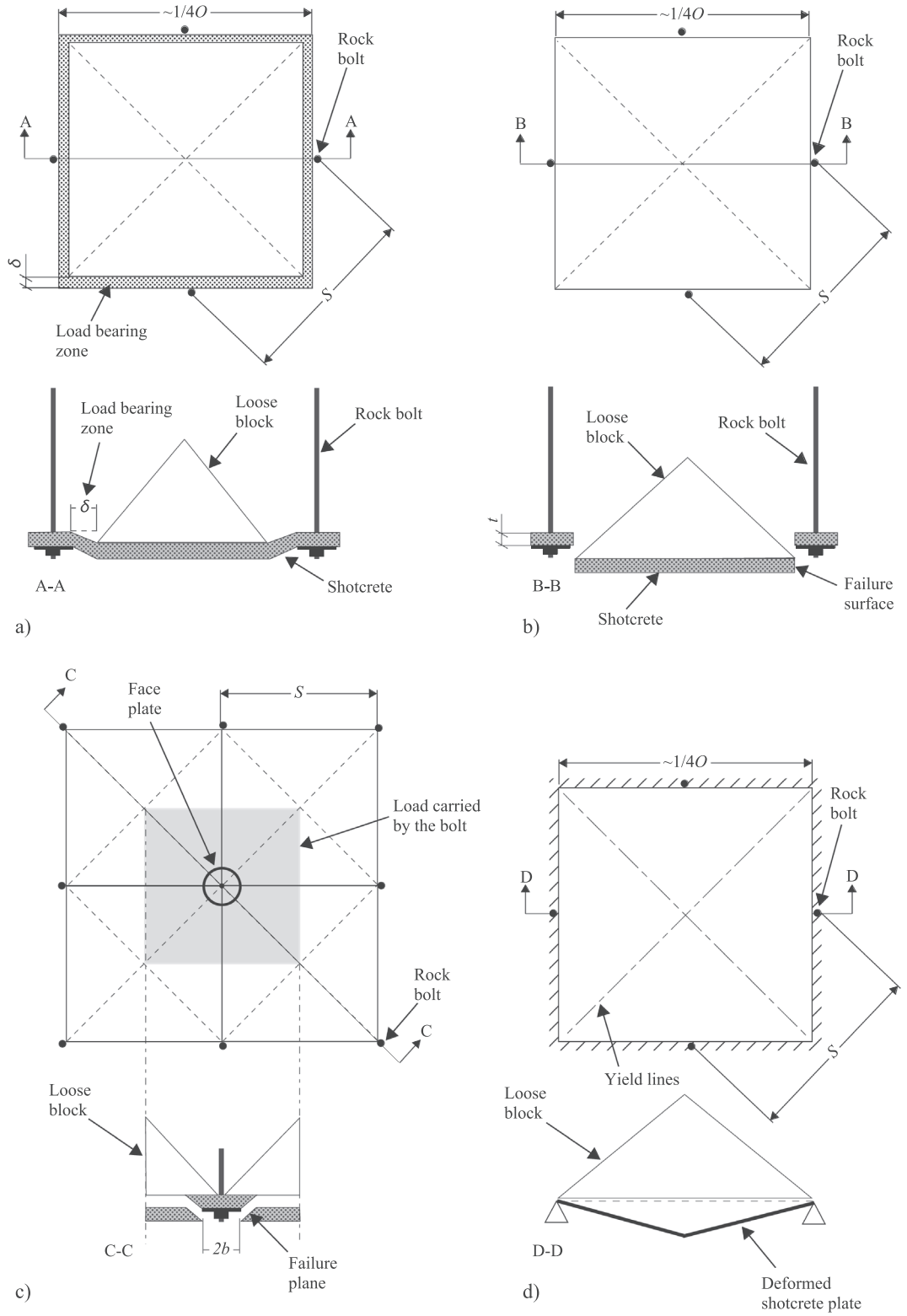

Fig. 1. Model of (a) Adhesive failure; (b) Direct shear failure; (c) Punching shear failure; (d) Flexural failure (© Bjureland et al., 2019, CC–BY 4.0, https://creativecommons.org/licenses/by/4.0).

assumption when doing so is that the load-bearing capacity of the shotcrete is governed by the spatial average of the input parameters (Holmgren, 1992; Barrett and McCreath, 1995; Banton et al., 2004; Lindfors et al., 2015). The spatial variability of the parameters is thereby commonly neglected and as a result, if the capacity is governed by the lowest value of a certain parameter, this assumption is non-conservative. It is therefore of significant importance to determine whether the spatial average of a shotcrete input parameter can be used to represent that parameter in design.

In this paper, we present a novel approach that can be used to account for the spatial variation of shotcrete thickness in both deterministic and reliability-based design of shotcrete. The approach is based

on results from numerical simulations of a shotcrete slab between rockbolts using Finite Element Methods, FEM. We investigate the effect that the spatially varying shotcrete thickness has on the flexural load-bearing capacity of a shotcrete slab. This choice was made since shotcrete thickness is one of the governing parameters in the determination of the flexural capacity and since the measurement methods available today, such as laser scanning using LiDAR (Light Detection and Ranging), allow for the possibility to quantify the shotcrete's spatial variability. Other authors have made a similar choice in related studies (Chang, 1994; Nilsson, 2003; Malmgren and Nordlund, 2008; Lee, 2010; Sjölander, 2017; Sjölander et al., 2017). In contrast to these authors, however, who as an example modeled the shotcrete as a sinusoidal wave-shaped shotcrete layer with rockbolts placed in the peaks of the shotcrete layer, we utilize shotcrete thickness data combined with random field theory (e.g. Vanmarcke, 1977) to describe the spatial variability of the shotcrete thickness. The data consisted of the statistical distribution of the thickness and its scale of fluctuation (i.e. the distance within which the magnitude of a parameter shows strong correlation with itself (Vanmarcke, 1977)) obtained from the Stockholm City Line project (Stockholm, Sweden) (Bjureland et al., 2019) and the Äspö Hardrock Laboratory tunnel (Oskarshamn, Sweden) (Klaube, 2018). Based on the results from our numerical simulations, a methodology is suggested how to account for the spatial variation of shotcrete thickness in both deterministic and reliability-based design of shotcrete. At the end of the paper, the implications of the results from this approach for shotcrete design are discussed.

2. General methodology

In order to investigate the influence from the spatial variability in shotcrete thickness, numerical calculations have been performed using the FEM software Abaqus (Hibbett et al., 1998). The numerical simulations can be divided into two main parts (Fig. 2). The first part essentially consists of setup, validation, and verification of the numerical model and the input parameters that are used to investigate the influence from the spatial variability in the shotcrete thickness (Sections 3.1–3.4). The second part essentially consists of the numerical calculations performed to investigate the influence from the spatial variability in shotcrete thickness.

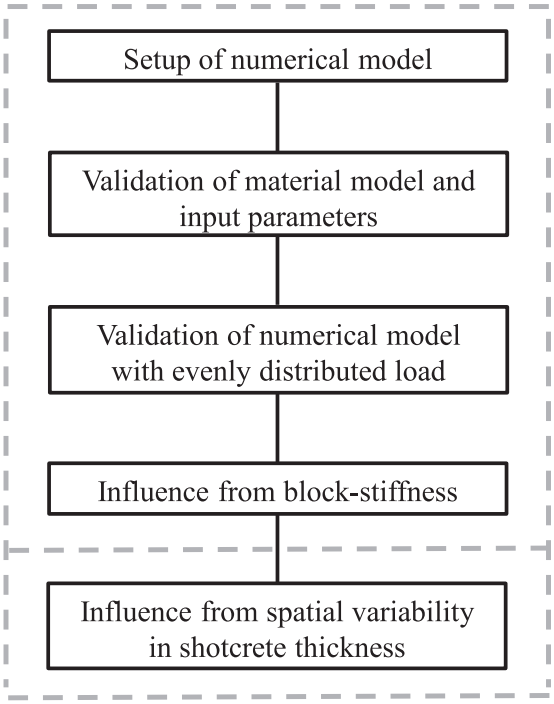

Fig. 2. Outline of the different parts in the analysis.

In the first part, a numerical model of a shotcrete slab was set up to simulate the flexural failure mode for a typical shotcrete roof support in a rock tunnel with a flat or moderately arched roof. A suitable material model was chosen for the slab and the required input parameters were defined.

To validate the material model and to calibrate the input parameters, the results from a numerical simulation of a four-point beam test (CEN, 2006a) were compared with the results from an experimental four-point beam test (Andersson, 2014).

To verify the numerical model, numerical calculations were conducted in which the shotcrete slab was subjected to an evenly distributed load, q. The results were compared with analytical calculations of a simply supported shotcrete slab exposed to the same q.

Since the stiffness of the load, i.e. the loose block, affects the load-bearing capacity of the shotcrete, numerical calculations were performed with different elastic moduli of the rock, E_R, to determine a suitable stiffness to use in the analysis performed in the second part. The same numerical model as previously was used, but instead of subjecting the slab to an evenly distributed load, the load was applied by assigning a prescribed displacement at the top of a rectangular block resting on the slab. The benefit of this approach is that the load is applied stepwise and thus "failure" of the shotcrete slab can be evaluated from the load-displacement curve. The E_R was varied between zero, which is equivalent to an evenly distributed load, and 10 GPa.

In the second part, to study the assumption that the spatial average of a parameter can be used to represent that parameter in design, a slab with an uneven bottom surface was first modelled using a varying shotcrete thickness, t, in accordance with a lognormal distribution $LN(\mu_t, \sigma_t, \theta_t)$, where μ_t is the mean value, σ_t is the standard deviation, and θ_t is the scale of fluctuation for the shotcrete thickness. In addition, two comparative evenly thick slabs were modeled: one with a thickness equal to the mean shotcrete thickness of the uneven slab, such that $t_{even} = \mu_t$, and one with a thickness equal to the mean shotcrete thickness of the uneven slab *along the periphery of the block*, such that $t_{even} = \mu_{tp}$. This choice was made since two different scenarios for spatial averaging are plausible (Fig. 3a and b).

In the first scenario, it can be assumed that the load-bearing capacity of a shotcrete layer with a spatially varying shotcrete thickness between four rockbolts is governed by μ_t. According to yield-line theory, it can in such a case be assumed that the yield lines are developed from the rockbolts towards the center of the area between the rockbolts and, thus, a large part of the shotcrete is involved in the failure. However, in the second scenario, if the loose block is relatively stiff and the shotcrete along the periphery of the block is relatively thin, it is reasonable to assume that yielding of the shotcrete layer is concentrated close to or at the periphery of the block. As a consequence, if the θ_t is equal to or smaller than the center-to-center distance between the rockbolts (i.e. the side length of the potential loose block), local zones of thick or thin shotcrete that do not affect its load-bearing capacity can exist in the center of the loose block (Fig. 3a and b). Therefore, in this scenario, it can be assumed that the load-bearing capacity of a shotcrete layer with a spatially varying t is governed by μ_{tp}.

The thickness variation in the uneven slab was modeled by randomly generating values from a predefined probability distribution $LN(\mu_t, \sigma_t, \theta_t)$ at a number of equally spaced points using random field theory. The assigned probability distribution was based on the work done by Bjureland et al. (2019), except for θ_t which was based on the work done by Klaube (2018). The boundary conditions, material model, and input parameters were the same as those defined in part one.

Both the uneven slab with $t \in LN(\mu_t, \sigma_t, \theta_t)$, and the two even slabs with $t_{even} = \mu_t$ and $t_{even} = \mu_{tp}$ were loaded by displacing the top of the same block as in part 1. The E_R used in the simulations was chosen based on the results from the fourth step in part one. The process of generating an uneven slab using random field theory, generating two

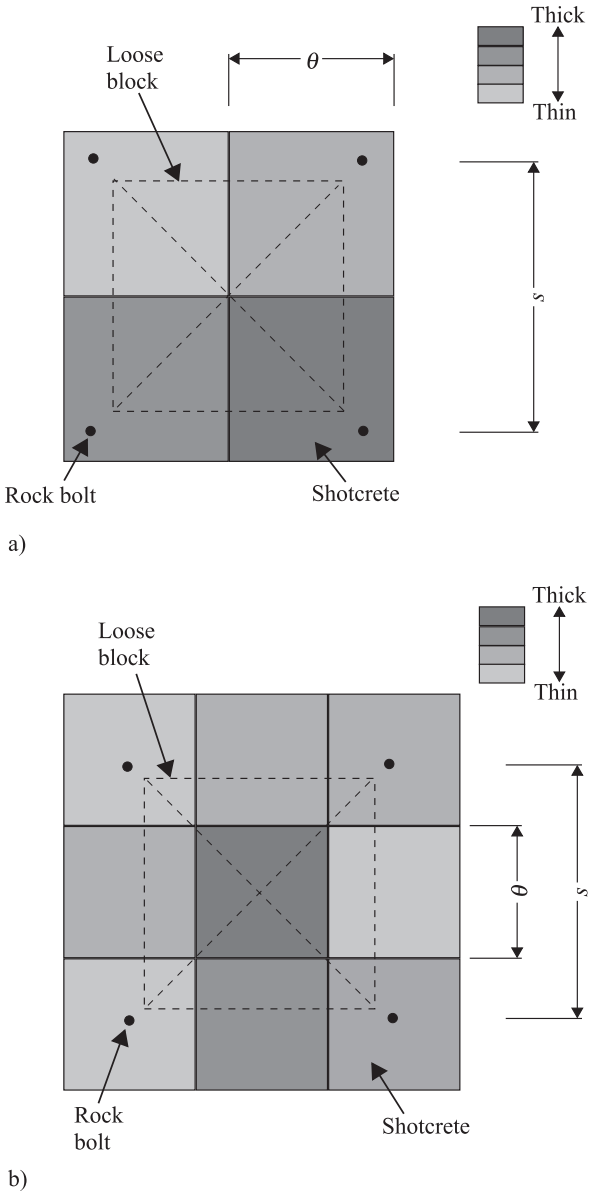

Fig. 3. Illustration of (a) the first scenario, in which the rock block between bolts is positioned in such a way that it is reasonable to assume that the load-bearing capacity is governed by μ_t; (b) the second scenario, in which the block is positioned in such a way that it is reasonable to assume that the thick layer of shotcrete in the center of the slab does not significantly affect its load-bearing capacity and therefore that the load-bearing capacity is governed by μ_{tp}.

comparative slabs with $t_{even} = \mu_t$ and $t_{even} = \mu_{tp}$, and subjecting all three slabs to the load from a block with a prescribed displacement were repeated ten times.

3. Set-up and validation of numerical model

3.1. Set-up of numerical model for the shotcrete slab

The numerical model of the shotcrete slab was set up in the FEM software Abaqus (Hibbett et al., 1998) using 10-noded quadratic tetrahedron (C3D10) continuum elements (Fig. 4). The thickness of the slab and the application of the load were varied for the different analyses (see Sections 3.3 and 4.1). Since we are investigating the influence from a spatially varying thickness on the flexural load-bearing capacity of shotcrete, we simplify the shotcrete support into a shotcrete slab with side length l = 1.7 m, which is supported along all edges. This

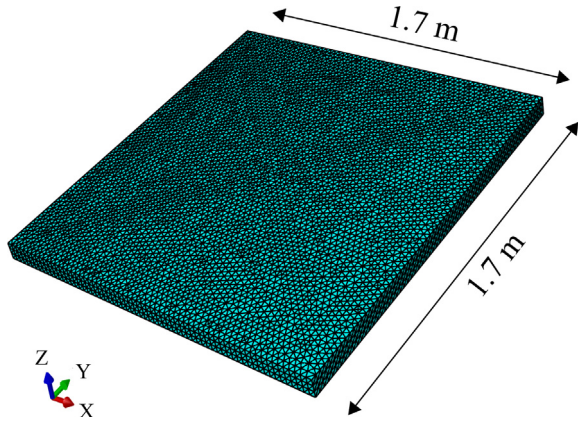

Fig. 4. Numerical model and finite element mesh of the slab used in the calculations performed in parts three and four.

represents a typical tunnel support with shotcrete and systematically installed rock bolts with a center to center distance of 1.7 m. Similar approaches were used by Holmgren (1992), Nilsson (2003), Diamantidis and Bernard (2004), and Bjureland et al. (2019). We made the conservative choice to model the slab as a simply supported slab by prohibiting all edges of the slab from moving vertically and horizontally along the direction of each edge. All edges were allowed to move horizontally towards the center of the slab and rotations were allowed in all directions of each edge.

Note here that the boundary conditions for shotcrete support between four rockbolts are complex, since the structural behavior of the slab is governed by a relationship between the stiffness of the rockbolts, the relative stiffness between the loose block and the shotcrete, the stiffness of the surrounding rock mass, and the interaction between the shotcrete and the rock mass outside the load-bearing zone illustrated in Fig. 1a. Defining this relationship is outside the scope of this paper and we therefore use the common approach (Holmgren, 1992; Barrett and McCreath, 1995; Nilsson, 2003; Diamantidis and Bernard, 2004; Bjureland et al., 2019), and make the aforementioned simplifying assumptions.

The material model used to describe the behavior of the shotcrete material in the simulations was the discrete crack approach model "Concrete Damage Plasticity" (Lubliner et al., 1989), implemented in Abaqus. The input parameters used in the analysis can be seen in Table 1. Similar parameters were used by Andersson (2014).

The post-failure non-linear tension softening behavior of the shotcrete was described using a bi-linear approach. The fracture energy, G_F, which is the parameter that mainly governs the post-failure behavior (Andersson, 2014), was estimated in accordance with the Model Code for unreinforced concrete to be (Beverly, 2013):

Table 1
Input parameters for the shotcrete model.

Name	Denotation	Magnitude	Unit
Modulus of elasticity	E_s	38.6	[GPa]
Poisson's ratio	ν_s	0.2	[–]
Unit weight	γ_s	23.0	[kN/m^3]
Uniaxial compressive strength	F_{cc}	58.0	[MPa]
Uniaxial tensile strength[a]	F_{ct}	4.1	[MPa]
Ultimate compressive strain	ε_{cu}	0.0034	[–]
Strain at maximum compressive stress[b]	ε_{c1}	0.0026	[–]
Maximum damage parameter	$d_{t,max}$	0.95	[–]

[a] First calculated based on point load at cracking from load–deflection curves and then adjusted by a factor 0.55 to match test curves (Andersson, 2014).
[b] In accordance with the Model Code for concrete class C50 (Beverly, 2013).

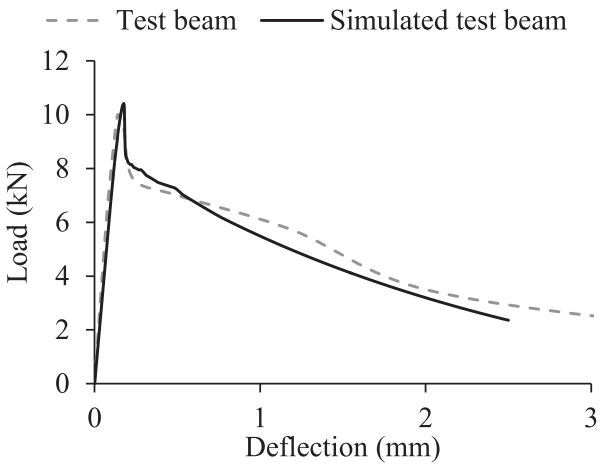

Fig. 5. Load–deflection curves for test beam and numerical simulation of the test beam.

$$G_F = 73\left(\frac{F_{cc}}{10^6}\right)^{0.18}. \quad (1)$$

The F_{cc} is the uniaxial compressive strength of the shotcrete in Pa. To account for the increase in G_F due to the fiber reinforcement in the shotcrete, the fracture energy of the fiber-reinforced shotcrete, $G_{F,FRS}$, was calculated as (Kazemi et al., 2007):

$$G_{F,FRS} = 10G_F. \quad (2)$$

3.2. Validation of shotcrete material model and input parameters

To validate the shotcrete material model and the input parameters, a four-point beam test (CEN, 2006a) was simulated in Abaqus using reduced integration plain stress elements, CPS4R. The results from the simulations were compared with an experimental four-point beam test conducted in accordance with CEN (2006a) (Andersson, 2014). The results from the experimental and the simulated four-point beam tests can be seen in Fig. 5.

3.3. Verification of the numerical model for the shotcrete slab

To verify the numerical model, numerical calculations were compared with analytical calculations of a simply supported shotcrete slab exposed to q using both idealized elastic and elastic–plastic conditions. In both of these verification calculations, the thickness was set to 75 mm. The slab consisted of 81,587 elements.

3.3.1. Elastic conditions

In the calculations in elastic conditions, verification of the numerical calculations was performed by comparing the analytical solution for the deflection at midspan, w_{max}, of a slab using Kirchhoff's plate theory (Timoshenko and Woinowsky-Krieger, 1959; Ventsel and Krauthammer, 2001):

$$w_{max} = 0.00416\frac{ql^4}{\left[\frac{E_S t^3}{12(1-\nu_S^2)}\right]}. \quad (3)$$

In the calculations in elastic conditions, a limitation in the magnitude of q was defined to ensure elastic conditions. The limitation of q was determined based on the elastic flexural capacity of the shotcrete slab, $R_{fl,e}$, (Barrett and McCreath, 1995; Banton et al., 2004):

$$R_{fl,e} = f_{ct}\frac{t^2}{6}, \quad (4)$$

in which f_{ct} is the shotcrete's flexural tensile strength at first crack, and the moment, M_e, calculated using Kirchhoff's plate theory (Timoshenko and Woinowsky-Krieger, 1959; Ventsel and Krauthammer, 2001):

$$M_e = 0.0469ql^2. \quad (5)$$

Table 2
Calculation results from the comparison between numerical and analytical calculations in elastic conditions.

Name	Denotation	Calculation	
		Analytical	Numerical
Deflection at midspan	w_{max}	0.737 mm	0.762 mm
Moment	M_e	4.07 kNm	3.84kNm

The f_{ct} was evaluated from the numerical test beam and equaled 4.39 MPa. The maximum q that could be used to ensure elastic conditions thus equaled 30.4 kPa. The q was therefore limited to 30 kPa in the calculations in elastic calculations. The results from these calculations can be seen in Table 2.

As can be seen in the table, the difference between the analytical and numerical calculations is approximately 3–5% for both deformations and moments. Since Kirchhoff's plate theory does not account for shear deformations, the results produced by the numerical simulations are considered to be reasonable.

3.3.2. Elastic-plastic conditions

To verify the results produced by the numerical model after exceeding the elastic limit, numerical calculations were performed using the same simply supported slab as for the calculations in elastic conditions, but with a stepwise increasing q until failure of the slab was obtained. Failure was defined as the point on the load–deflection curve at which the derivative of the curve became either zero or negative.

The results from the numerical simulations were compared with analytical calculations using the maximum moment that the shotcrete could sustain, M_p, evaluated based on yield line theory and the maximum capacity of the shotcrete slab, $R_{fl,p}$, as suggested by Holmgren (1992):

$$M_p = \frac{ql^2}{24}, \quad (6)$$

$$R_{fl,p} = 0.9\frac{R_{10/5} + R_{30/10}}{200}\frac{f_{ct}t^2}{6}, \quad (7)$$

in which the factor 0.9 is introduced to account for the overestimation of $R_{fl,p}$ that Eq. (7) otherwise gives at small deflections for a shotcrete with a relatively high residual strength. The $R_{10/5}$ and $R_{30/10}$ are flexural toughness factors (ASTM, 1997) that adjust the moment capacity of the shotcrete to account for its residual strength. They can be determined from

$$R_{10/5} = 20(I_{10} - I_5), \quad (8)$$

and

$$R_{30/10} = 5(I_{30} - I_{10}), \quad (9)$$

in which I_5, I_{10}, I_{30} are ductility indexes, which are defined as the area underneath the load–deflection curve from a four-point beam test up to a certain deflection, δ, divided by the area underneath the curve up to the deflection at first crack, δ_S. The points to which the areas are calculated for are $I_5 = 3.0\delta_S$, $I_{10} = 5.5\delta_S$, and $I_{30} = 15.5\delta_S$.

For an elastic perfectly plastic material, both $R_{10/5}$ and $R_{30/10}$ are equal to 100. For the shotcrete used in this paper, $R_{10/5}$ and $R_{30/10}$ were determined based on the normalized numerically simulated test beam (Fig. 6) and equaled 162.2 and 185.4, respectively.

The maximum distributed load obtained from the elastic–plastic analytical calculations, $q_{max,a}$, = 53.6 kPa using Eqs. (6) and (7) and maximum distributed load obtained from the numerical calculations, $q_{max,n}$ = 65.0 kPa. As can be noted, the calculated $q_{max,n}$ is

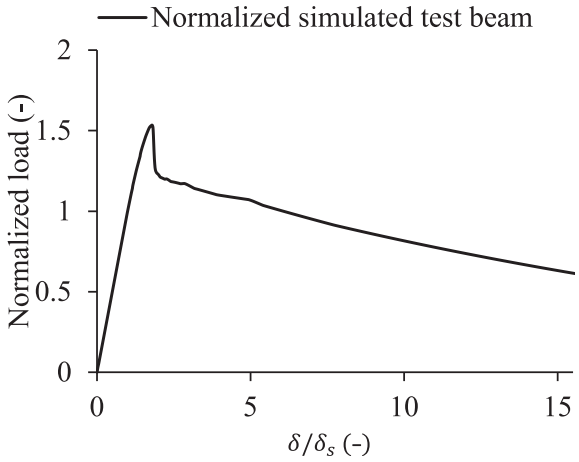

Fig. 6. Normalized load–deflection curve for the numerically simulated test beam.

approximately 20% higher than the calculated $q_{max,a}$. Probable reasons for obtaining a higher capacity from the numerical simulations are that the analytical calculations include $(R_{10/5} + R_{30/10})/200$, which is basically an averaging of the residual capacities (Holmgren, 1992), and also the 10% reduction made in Eq. (7) to account for potential overestimation of $R_{fl,p}$. If this reduction is neglected, the q_{max} obtained from the$q_{max,a}$ = 59.6 kPa and thus the difference between the analytical and numerical results is approximately 10%. Due to the above and the fact that the numerical calculations account for shear deformations, which reduces the moment and therefore increases the load-bearing capacity, the results are considered to be reasonable.

3.4. Determination of suitable block stiffness

Since the stiffness of the block affects the load-bearing capacity of the shotcrete, numerical simulations were performed using the same numerical model as in Section 3.3.2 to determine a suitable block stiffness to use in the forthcoming analysis in Section 4. However, instead of applying a distributed load to the shotcrete slab, the load was applied as a prescribed displacement at the top of a rectangular block with a base area of 1.5x1.5 m^2 and a height of 1.0 m (Fig. 7). The choice of using a rectangular shaped block, instead of a pyramidal shaped block as principally illustrated in Fig. 1d, was made to ensure that the results from the simulations in which small E_R are used are comparable with the commonly made assumption that the weight of the block is evenly distributed over the shotcrete slab (Eq. (6)). In addition, this choice was made to avoid the numerical difficulties that arises close to

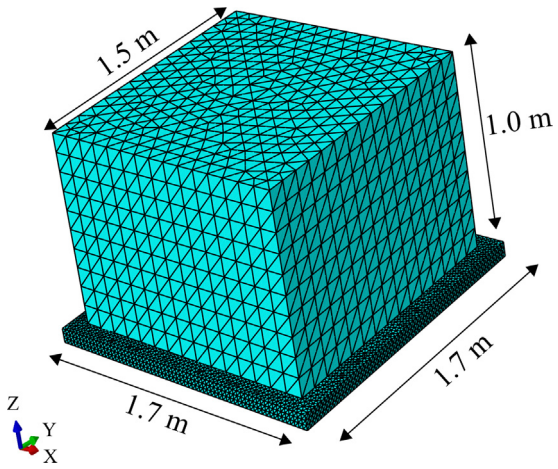

Fig. 7. Numerical model and finite element mesh of the slab and the block.

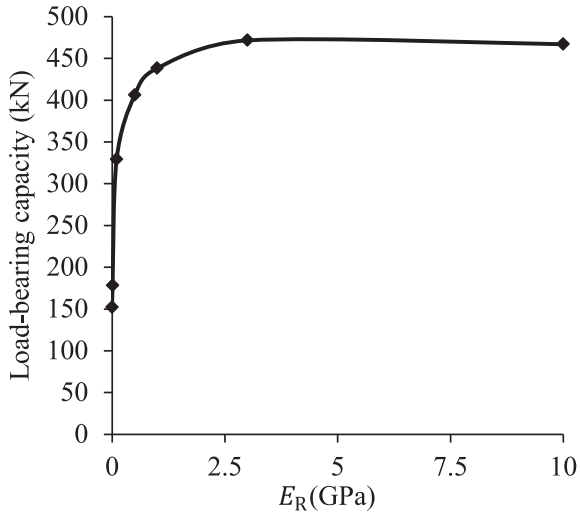

Fig. 8. Effect of the block's elastic modulus, E_R, on the slab's load-bearing capacity.

the edges of a pyramidal shaped block, where the height of the block is essentially zero, when assigning a prescribed displacement on the top-surfaces of the block. The base area was purposely decided to be smaller than the slab to avoid numerical difficulties arising from assigning opposing prescribed deformations along the edges of the slab. The size of the base area was selected such that it simulates a block that would fit between the edges of the face-plates of the rockbolts. The height of the block was set to be 1.0 m to allow analysis of the influence of the block stiffness on the load-bearing capacity of the shotcrete. The self-weight of the block was set to zero. The sides of the block were prevented from deforming horizontally. The rock mass that constitutes the block was modeled as a linearly elastic material with an E_R that was varied between zero and 10 GPa between the simulations. The Poisson's ratio of the rock mass, ν_r, was set to 0.25. The number of elements in the block was 15,228.

The results from the analyses can be seen in Fig. 8. As expected, the block stiffness had a substantial effect on the load-bearing capacity of the shotcrete. For a block with $E_R > 3$ GPa the load-bearing capacity of the shotcrete is approximately three times greater than that for a block with $E_R = 0$ GPa. This increase in load-bearing capacity is due to the stiffer block's capability to transfer the load from the center of the slab towards the circumference of the block, and as a result the load is transferred closer to the supporting edges of the slab.

To select a suitable block stiffness to use in the forthcoming analysis in Section 4, the E_R was estimated using RMR. For the flexural load-bearing capacity of shotcrete exposed to single loose blocks, the relevant RMR is approximately 30–70 (Banton et al., 2004; Lindfors et al., 2009). To estimate E_R, the relationships proposed by Bieniawski (1978) and Serafim and Pereira (1983) (Eq.10), respectively, were used:

$$E_R\,(\mathrm{GPa}) = \begin{cases} 2\mathrm{RMR} - 100, & \text{for } \&\mathrm{RMR} > 50 \\ 10^{(\mathrm{RMR}-10)/40}, & \text{for } \&\mathrm{RMR} > 30 \end{cases}. \quad (10)$$

Using these relationships, the E_R was calculated to be approximately 3–40 GPa, neglecting the infinitesimal E_R that the relationship by Bieniawski (1978) yields for RMR close to 50. Considering the fact that the load-bearing capacity is fairly constant over this entire spectrum of block stiffness (Fig. 8), we used an E_R of the rock mass equal to 3 GPa in the analysis in Section 4.

It should be noted here that the actual magnitude of E_R at which it has an effect on the load-bearing capacity of the shotcrete is related to the stiffness of the shotcrete slab, i.e. it is the relative stiffness between E_R and the stiffness of the shotcrete that governs the effect on the load-bearing capacity and not the actual magnitude of E_R. Therefore, if the

stiffness of the shotcrete support is changed, the magnitude of E_R at which it has an effect on the load-bearing capacity changes. This must be accounted for when designing tunnel support.

4. Influence on shotcrete's flexural load-bearing capacity from spatial variability of shotcrete thickness

4.1. Numerical model and calculation procedure

To simulate an uneven shotcrete slab, a random field was generated using the statistical software R! (Homik, 2006) and its Random Fields package (Schlater, 2001). This choice was made since random field theory is a stringent approach to simulate spatial variability by incorporating its defining characteristics in a mathematical idealization. The random field was defined as a stationary Gaussian random field using the midpoint method. As such, the mean and covariance were assumed to be constant over the entire random field, the correlation function was assumed to be Gaussian, and the value of the variable simulated, i.e. t, was represented by the value at the center of each of the elements that the random field constitutes of (e.g. Hajializadeh et al., 2016). Similar choices have been made by other authors (e.g. Li and Der Kiureghian, 1993; Haldar and Mahadevan, 2000; Malioka and Faber, 2004; Stewart and Mullard, 2007; Krounis et al., 2015; Shi and Stewart, 2015). The element size in the random field was set to 0.1 m consistently over the entire random field to avoid mathematical difficulties (Der Kiureghian and Ke, 1988; Fenton and Griffiths, 2008; Shi and Stewart, 2015).

To generate a random field, the mean and standard deviation together with its statistical distributions and the scale of fluctuation for the parameter of interest must be known. For t within the area of four rockbolts, none of these parameters have been quantified in the available literature. Bjureland et al. (2019), however, illustrated that the variation in t in a newly constructed commuter train tunnel in Stockholm, Sweden, followed a lognormal distribution over a large part of the entire tunnel and that the COV was approximately 32% for a shotcrete thickness requirement of 75 mm. In addition, Klaube (2018) illustrated that in a part of the Äspö Hardrock Laboratory tunnel in Oskarshamn, Sweden, θ_t was equal to approximately 0.8 m. Therefore, for the generation of the random field in this paper, the t was assumed to follow a lognormal distribution withμ_t = 75 mm and a COV of 32% and the θ_t was assumed to be 0.8 m. Since the random field was defined as Gaussian, the above-described lognormal distribution was transformed to the corresponding normal distribution. Following the transformation, the random field was generated and the value obtained in each element was then back-transformed to the lognormal distribution. A similar procedure was used by Krounis et al. (2015). The parameters used for the random fields can be seen in Table 3.

Because of the lack of studies on the magnitude of θ_t, it is assumed in this paper that the θ_t quantified at Äspö Hardrock Laboratory tunnel is representative for θ_t in the City Line Project, even though the conditions at Äspö Hardrock Laboratory are not exactly the same as those in the City Line Project.

Table 3
Parameters used for random fields.

Parameter	Magnitude
Random field style	Stationary
Correlation function	Gaussian
Scale of fluctuation, θ_t	0.80 m
Element size	0.10 m
Mean[c]	−2.6 m
Variance[c]	0.098 m^2

[c] The mean and variance provided in the table are after transformation from the lognormal distribution. The corresponding untransformed values for the mean and variance equals 0.075 m and 0.00058 m^2.

The analysis performed in this section can be summarized into the following steps:

(a) The lognormal distribution for t suggested by Bjureland et al. (2019) was transformed into the corresponding normal distribution.
(b) Spatially varying values for t using the transformed distribution and the θ_t suggested by Klaube (2018) were randomly generated at points spaced 0.1 m over the entire 1.7x1.7 m^2 slab.
(c) The randomly generated values for t at each of the 0.1 m spaced points were back-transformed to the lognormal distribution.
(d) The geometry of a 3D slab with an even top surface and an uneven bottom surface was created in Autodesk Civil 3D. The unevenness of the bottom surface, and thus the variation in t throughout the slab, were created by importing the spatially varying values of t obtained in step (c) as a point cloud into Autodesk Civil 3D and generating a 3D slab from that point cloud.
(e) The 3D slab created in (d) was imported as a structural part into the numerical model in Abaqus.
(f) The μ_t and the μ_{tp} were calculated based on the values obtained in (c).
(g) Both an evenly thick comparative slab using the calculated μ_t from step (f) and an evenly thick comparative slab using the calculated μ_{tp} from step (f) were created in Abaqus.
(h) The boundary conditions for each of the three slabs were defined in accordance with that described in Section 3.1.
(i) One simulation for each of the three slabs created in steps (d)–(g) was performed using the block geometry, the E_R, and the prescribed displacement described in Section 3.4.
(j) The load-bearing capacity obtained from the simulation of the uneven slab was extracted and compared with the load-bearing capacities obtained and extracted from both of the simulations of the even slabs with $t_{even} = \mu_t$ and $t_{even} = \mu_{tp}$.
(k) Steps (b)–(j) were repeated ten times.

4.2. Results

The obtained load-bearing capacity from each simulation can be seen in Fig. 9a–b. In most of the performed analyses the load-bearing capacity of the uneven slab is approximately the same as that for an even slab with $t_{even} = \mu_t$. The discrepancy is within approximately 10%. However, an exception is found for the evenly thick slab with the highest load-bearing capacity (i.e. the point furthest to the right in Fig. 9a, simulation number 4) in which the difference in load-bearing capacity between the slabs is 28%.

As can also be seen in Fig. 9a–b, in most of the analyses the load-bearing capacity for the uneven slabs is better estimated using an even slab with $t_{even} = \mu_t$ than a $t_{even} = \mu_{tp}$. However, some exceptions exist such as the load-bearing capacity estimated in simulation number 4, in which the load-bearing capacity of the uneven slab is approximately the same as the load-bearing capacity of an even slab with $t_{even} = \mu_{tp}$ (i.e. the point with the third highest load-bearing capacity of the uneven slabs in Fig. 9b).

5. Discussion

One reason for obtaining the results presented in Section 4.2 is the probability of having a local zone with thin or thick shotcrete at the center of the loose block (Fig. 3a–b). Taking the results from simulation number 4 as an example, the discrepancy in load-bearing capacity between the uneven slab and the even slab with $t_{even} = \mu_t$ is because of a local large thickness zone at the center of the slab. In addition, three of the uneven slab's corners are relatively thin locally. As a consequence, μ_t in the slab used in simulation 4 is considerably larger than μ_{tp}. In all other simulations, the uneven slab consists of zones with thin or thick

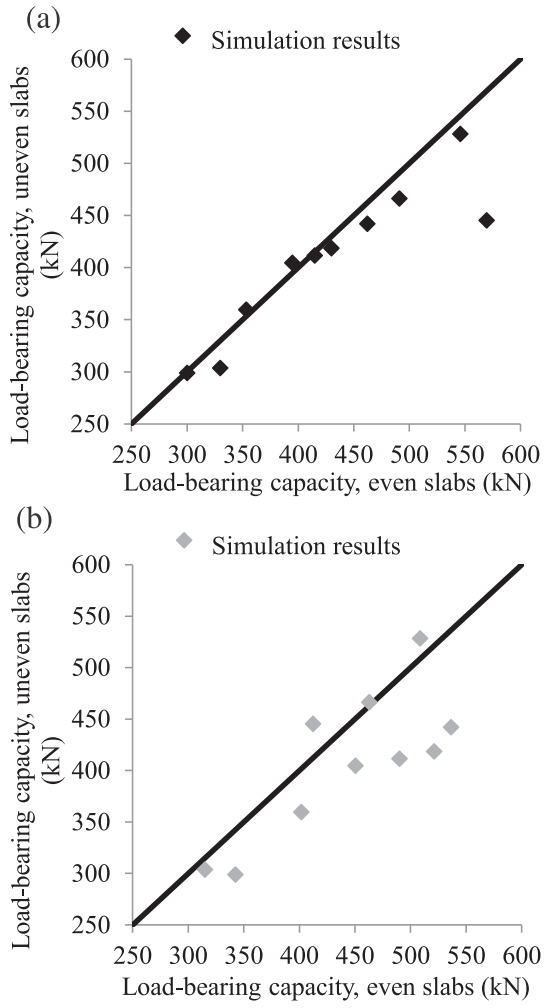

Fig. 9. The load required to reach failure for the even and uneven shotcrete slabs. In (a) the thickness of the even slab is equal to the mean thickness of the entire uneven slab ($t_{even} = \mu_t$). In (b) the thickness of the even slab is equal to the mean thickness of the uneven slab along the periphery of the block ($t_{even} = \mu_{tp}$).

shotcrete spread out across the entire slab, which results in a smaller difference between μ_t and μ_{tp}.

The effect of this geometrical difference is a change in the distribution of stresses and thus the development of maximum principal plastic strains. In simulation number 4, the maximum principal plastic strains are initiated at the three corners of the block, where the slab is relatively thin, and are afterwards distributed towards the corners of the slab and simultaneously along the periphery of the block (Fig. 10a–d). For all other slabs, the maximum principal plastic strains are initiated at the corners and are afterwards distributed towards the center of the slab (Fig. 11a–d). The consequence is that using μ_t as t in Eq. (7) to estimate the load-bearing capacity of a slab might lead to an overestimation in load-bearing capacity.

These results illustrate that neither of the two described scenarios is valid in all cases. Determination of a slab's flexural load-bearing capacity is more complex than simply assuming that it is governed by either μ_t or μ_{tp}. If the minimum load-bearing capacity of an even slab with $t_{even} = \mu_t$ or $t_{even} = \mu_{tp}$ is used, however, good agreement is obtained for the load-bearing capacity between the uneven slab and the even slab (Fig. 12). A possible approach to use in practical design of shotcrete would therefore be to estimate the load-bearing capacity of the uneven slab based on the minimum load-bearing capacity of an even slab calculated with μ_t or with μ_{tp}. By doing so, the spatial variability of shotcrete thickness can be accounted for in analytical reliability-based design calculations. Before using this approach, however, some important aspects need to be further addressed.

First, the suggested approach for practical design requires the engineer to have knowledge about the probability distribution of the shotcrete thickness and its mean, variance, and scale of fluctuation. It also requires that this knowledge be used to generate random fields that properly represent the spatial variability of shotcrete thickness. In this paper, we use the variance and probability distribution provided by Bjureland et al. (2019) and the scale of fluctuation provided by Klaube (2018) to generate the random fields, all of which were proposed based on data obtained from relatively large parts of two tunnels. As such, the mean, the variance, the probability distribution, and the scale of fluctuation used in this paper do not necessarily describe the variability of the shotcrete thickness within the area of four rockbolts in general. Determining these parameters for shotcrete thickness in other tunnel projects under different types of geological conditions is therefore necessary.

Second, we have only studied the influence of spatial variability in shotcrete thickness on the load-bearing capacity of the shotcrete. In reality, spatial variability of other parameters such as adhesion between rock and shotcrete, shear strength, and flexural strength of the shotcrete might also affect the load-bearing capacity.

Last, if the minimum load-bearing capacity obtained using μ_t and μ_{tp} is used in the design of shotcrete support, an essential part of the design is to specify suitable control measures that capture all critical information. For shotcrete thickness, the standardized control method in European countries consists of drilling five holes spaced 600 ± 50 mm apart in two lines of three holes at right angles sharing the center hole (CEN, 2006b). This procedure is repeated at random locations on the shotcrete surface in the tunnel. Considering that this method of verifying the design captures neither the variance within four rockbolts nor the scale of fluctuation, the critical information required for verification of the design is not obtained. Therefore, since measurement methods such as LiDAR which can capture the critical information are available, it would be preferable to adjust the standardized control measures and include these methods in such a way that the critical information is captured.

6. Conclusions

Using the spatial average of shotcrete thickness between four rockbolts to represent shotcrete thickness in design can result in an overestimation of the shotcrete's flexural load-bearing capacity. The spatial variability of shotcrete thickness therefore needs to be accounted for. We have shown that by using the minimum of: (1) the spatial average thickness of a shotcrete slab of varying thickness, or (2) the spatial average thickness of the slab along the periphery of the loose block, the spatial variability of shotcrete thickness can be accounted for in practical design of shotcrete support without the use of complex and time-consuming numerical calculations.

CRediT authorship contribution statement

William Bjureland: Conceptualization, Methodology, Validation, Formal analysis, Writing - original draft, Visualization. **Fredrik Johansson:** Conceptualization, Methodology, Resources, Writing - review & editing, Supervision, Project administration, Funding acquisition. **Johan Spross:** Conceptualization, Methodology, Writing - review & editing, Supervision. **Stefan Larsson:** Conceptualization, Resources, Writing - review & editing, Supervision, Project administration, Funding acquisition.

Declaration of Competing Interest

The authors declare that they have no known competing financial

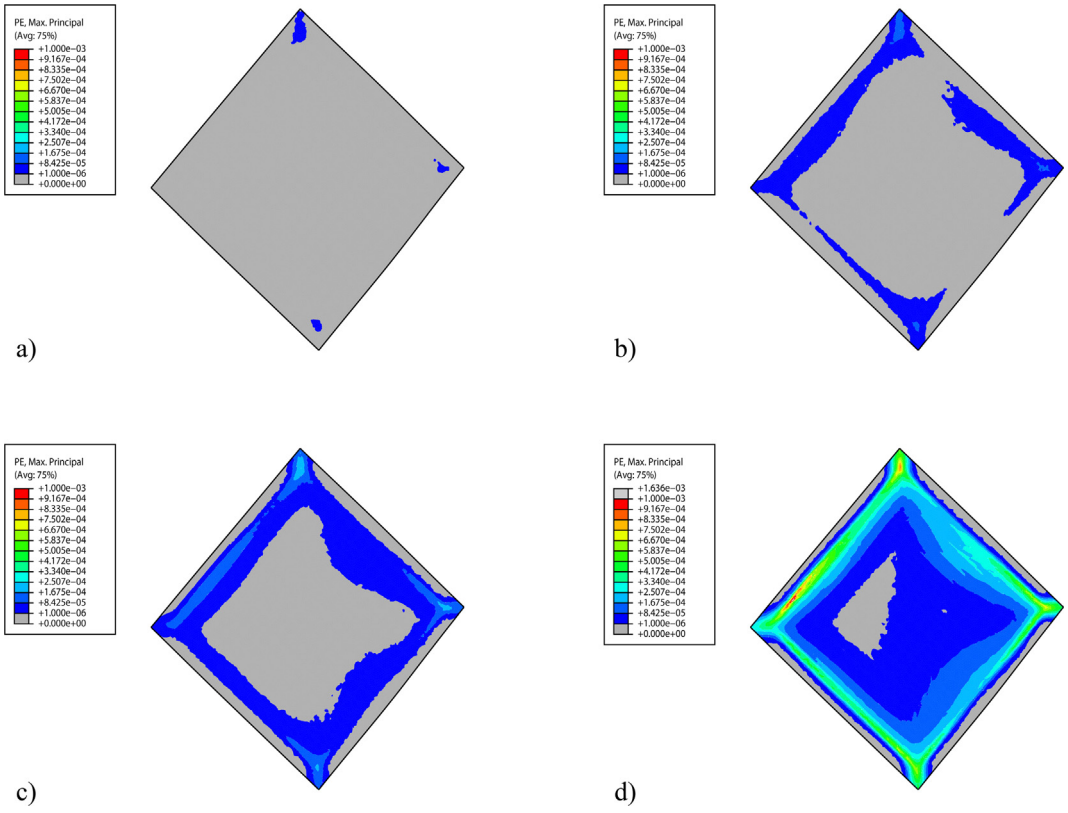

Fig. 10. a-d) Illustration of how plastic strains are initiated at the corners of the block and then stretch towards the corners of the slab and along the periphery of the block.

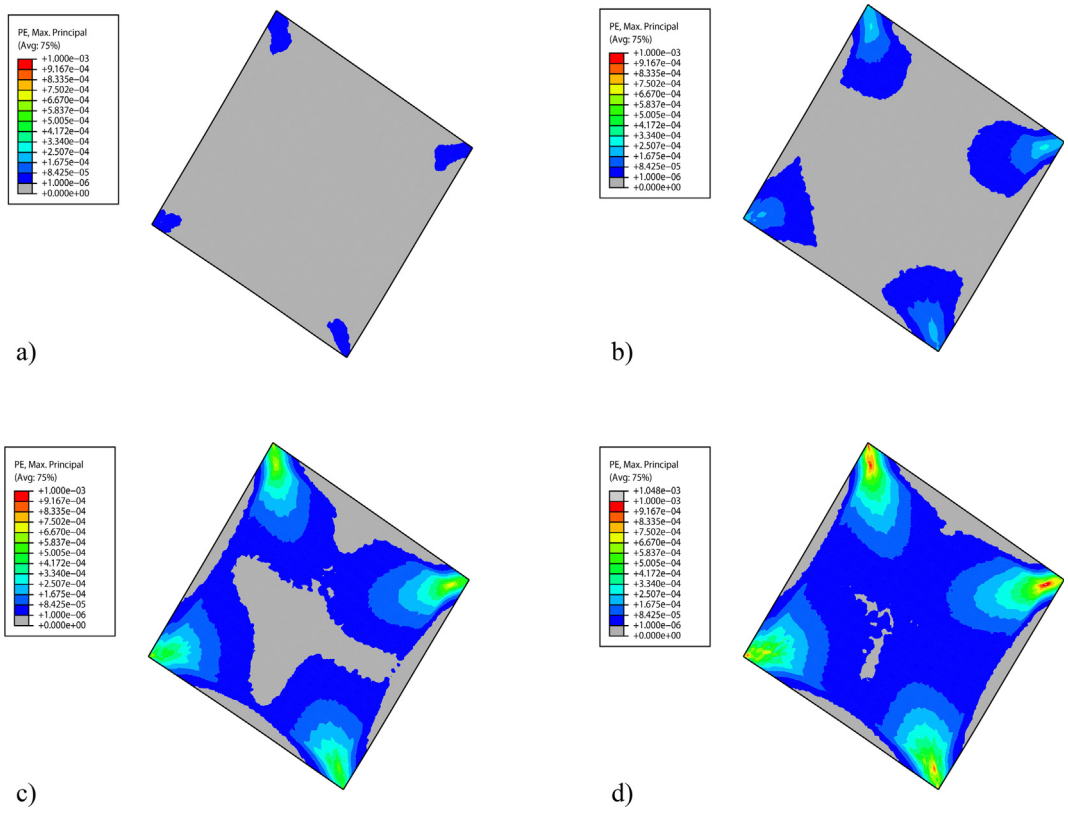

Fig. 11. (a–d) Illustration of how plastic strains are initiated at the corners of the block and then stretch towards the corners of the slab and the center of the slab.

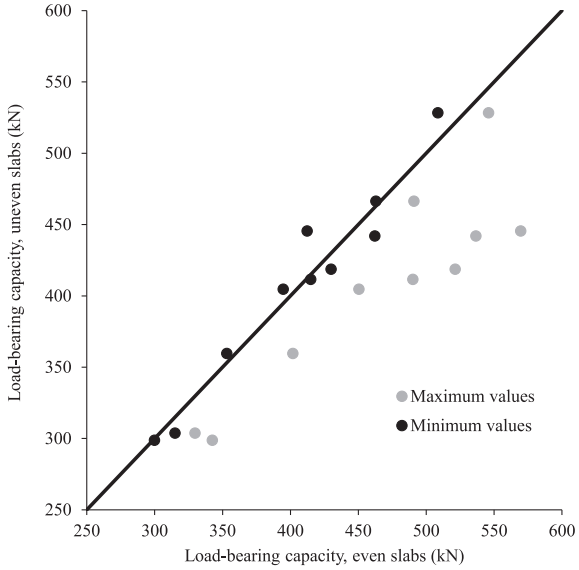

Fig. 12. The load required to reach failure for the even and uneven shotcrete slabs. The shotcrete thicknesses, t, of the two even slabs are $t_{even} = \mu_t$ and $t_{even} = \mu_{tp}$, respectively. Black-colored circles represent the minimum load-bearing capacity for each simulation pair of slabs with thicknesses μ_t and μ_{tp}. Gray-colored circles represent the maximum load-bearing capacity for each simulation pair.

interests or personal relationships that could have appeared to influence the work reported in this paper.

Acknowledgements

The authors acknowledge the funders of the TRUST project (www.trust-geoinfra.se) for their support of the research presented: the Rock Engineering Research Foundation, BESAB, SBUF, SKB (the Swedish Nuclear Fuel and Waste Management Co), and SVC (Swedish Hydropower Center, www.svc.nu). SVC has been established by the Swedish Energy Agency, Elforsk and Svenska Kraftnät together with Luleå University, KTH Royal Institute of Technology, Chalmers University of Technology, and Uppsala University.

Appendix A. Supplementary material

Supplementary data to this article can be found online at https://doi.org/10.1016/j.tust.2020.103336.

References

Andersson, A., 2014. Impact Loading on Concrete Slabs: Experimental Tests and Numerical Simulations, Report 153. KTH Royal Institute of Technology, Stockholm.
ASTM, 1997. 1018: Standard Test Method for Flexural Toughness and First-crack Strength of Fiber-reinforced Concrete (using beam with third-point loading). American Society of Testing Materials, West Conshohocken, USA.
Bagheri, M., 2011. Block Stability Analysis using Deterministic and Probabilistic Methods. PhD thesis, TRITA–JOB 1016. KTH Royal Insitute of Technology, Stockholm.
Banton, C., Diederichs, M., Hutchinson, D., Espley, S., 2004. Mechanisms of shotcrete roof support. In: Balkema, A.A. (Ed.), 2nd International Conference on Engineering Developments in Shotcrete, Leiden, London, pp. 39–46.
Barrett, S., McCreath, D., 1995. Shortcrete support design in blocky ground: Towards a deterministic approach. Tunn. Undergr. Sp. Techn. 10, 79–89.
Bernard, E., Xu, G., 2017. Influence of fibre count on variability in post-crack performance of fibre reinforced concrete. Mater. Struct. 50, 169.
Bernard, E., Xu, G., 2019. Normality of post-crack performance data for fiber-reinforced concrete. Adv. Civ. Eng. 8, 145–157.
Beverly, P., 2013. Fib Model Code for Concrete Structures 2010. Ernst & Sohn, Berlin.
Bieniawski, Z., 1978. Determining rock mass deformability: experience from case histories. Int. J. Rock. Mech. Min. Sci. Geomech. Abstr. 15, 237–247.
Bjureland, W., Johansson, F., Sjölander, A., Spross, J., Larsson, S., 2019. Probability distributions of shotcrete parameters for reliability-based analyses of rock tunnel support. Tunn. Undergr. Sp. Techn. 87, 15–26.
Bjureland, W., Spross, J., Johansson, F., Prästings, A., Larsson, S., 2017. Reliability aspects of rock tunnel design with the observational method. Int. J. Rock. Mech. Min. 98, 102–110.
Celestino, T.B., Aoki, N., Silva, R.M., Gomes, R.A.M.P., Bortolucci, A.A., Ferreira, D.A., 2006. Evaluation of tunnel support structure reliability. Tunn. Undergr. Sp. Tech. 21, 311.
CEN, 2002. EN 1990 – Basis of Structural Design. European Committee for Standardization, Brussels.
CEN, 2006a. EN 14488–3:2006 Testing Sprayed Concrete – Part 3: Flexural Strengths (first peak, ultimate and residual) of Fibre Reinforced Beam Specimens. European Committee for Standardization, Brussels.
CEN, 2006b. EN 14488–6:2006 Testing Sprayed Concrete – Part 6: Thickness of Concrete on a Substrate. European Committee for Standardization, Brussels.
Chang, Y., 1994. Tunnel Support with Shotcrete in Weak Rock – A Rock Mechanics Study. PhD thesis. KTH. Royal Institute of Technology, Stockholm.
Der Kiureghian, A., Ke, J.-B., 1988. The stochastic finite element method in structural reliability. Probabilist Eng. Mech. 3, 83–91.
Diamantidis, D., Bernard, E., 2004. Reliability-based resistance design of FRS tunnel linings. Shotcrete: More Eng. Dev. 12, 109–126.
Fenton, G.A., Griffiths, D.V., 2008. Risk Assessment in Geotechnical Engineering. John Wiley & Sons, Chichester.
Hajializadeh, D., Stewart, M.G., Enright, B., OBrien, E., 2016. Spatial time-dependent reliability analysis of reinforced concrete slab bridges subject to realistic traffic loading. Struct. Infrastruct. E. 12, 1137–1152.
Haldar, A., Mahadevan, S., 2000. Reliability Assessment using Stochastic Finite Element Analysis. John Wiley & Sons, Chichester.
Hibbett, Karlsson, Sorensen, 1998. ABAQUS/standard: User's manual. Hibbitt, Karlsson & Sorensen.
Holmgren, J., 1979. Punch-loaded Shotcrete Linings on Hard Rock. BeFo, Stockholm.
Holmgren, J., 1987. Bolt-anchored, steel-fibre-reinforced shotcrete linings. Tunn. Undergr. Sp. Tech. 2, 319–333.
Holmgren, J., 1992. Bergförstärkning med sprutbetong (Rock support with shotcrete, in Swedish). Vattenfall, Stockholm.
Homik, 2006. The R FAQ, http://cran.r-project.org (accessed 2019-12-16).
Jimenez-Rodriguez, R., Sitar, N., 2007. Rock wedge stability analysis using system reliability methods. Rock Mech. Rock Eng. 40, 419–427.
Jimenez-Rodriguez, R., Sitar, N., Chacon, J., 2006. System reliability approach to rock slope stability. Int. J. Rock Mech. Min. 43, 847–859.
Kazemi, M., Fazileh, F., Ebrahiminezhad, M., 2007. Cohesive crack model and fracture energy of steel-fiber-reinforced-concrete notched cylindrical specimens. J. Mat. Civil Eng. 19, 884–890.
Klaube, M., 2018. Spatial Variability of Shotcrete Thickness. MSc thesis, TRITA–ABE–MBT 188. KTH Royal Institute of Technology, Stockholm.
Krounis, A., Johansson, F., Larsson, S., 2015. Effects of spatial variation in cohesion over the concrete-rock interface on dam sliding stability. J. Rock Mech. Geotech. Eng. 7, 659–667.
Langford, J.C., 2013. Application of Reliability Methods to the Design of Underground Structures. PhD thesis. Queens University, Kingston, Ontario.
Lee, S.-D., 2010. Numerical analysis for irregular shotcrete on uneven tunnel perimeter. Int. J. Rock Mech. Min. 47, 488–495.
Li, C.-C., Der Kiureghian, A., 1993. Optimal discretization of random fields. J. Eng. Mech. 119, 1136–1154.
Lindfors, U., Rosengren, L., Von Matern, M., 2009. Design of standard reinforcement classes for a new commuter train tunnel in Stockholm. In: Proceedings of sinorock 09, Hong Kong.
Lindfors, U., Swindell, R., Rosengren, L., Holmberg, M., Sjöberg, J., 2015. Projektering av bergkonstruktioner (Design of rock engineering structures, in Swedish). Swedish Transport Administration, Stockholm.
Low, B.K., Einstein, H.H., 2013. Reliability analysis of roof wedges and rockbolt forces in tunnels. Tunn. Undergr. Sp. Tech. 38, 1–10.
Lubliner, J., Oliver, J., Oller, S., Onate, E., 1989. A plastic-damage model for concrete. Int. J. Solids Struct. 25, 299–326.
Lü, Q., Chan, C.L., Low, B.K., 2013. System reliability assessment for a rock tunnel with multiple failure modes. Rock Mech. Rock Eng. 46, 821–833.
Malioka, V., Faber, M., 2004. Modeling of the Spatial Variability for Concrete Structures. Aalborg University, Aalborg.
Malmgren, L., Nordlund, E., 2008. Interaction of shotcrete with rock and rock bolts—a numerical study. Int. J. Rock Mech. Min. 45, 538–553.
Matarawi, A.E., Harrison, J.P., 2017. Calibrated partial factors for support of wedges exposed in tunnels. Procedia Eng. 191, 802–810.
Napa-García, G.F., Beck, A.T., Celestino, T.B., 2017. Reliability analyses of underground openings with the point estimate method. Tunn. Undergr. Sp. Tech. 64, 154–163.
Nilsson, U., 2003. Structural Behaviour of Fibre Reinforced Sprayed Concrete Anchored in Rock. PhD thesis, TRITA–BKN 71. KTH. Royal Institute of Technology, Stockholm.
Schlater, M., 2001. Simulation of stationary and isotropic random fields. R-news 1, 18–20.
Serafim, J.L., Pereira, J.P., 1983. Consideration of the geomechanical classification of Bieniawski. In: Proc. Int. Symp. on Engineering Geology and Underground Construction. LNEC, Lisbon, pp. 33–44.
Shi, Y., Stewart, M.G., 2015. Spatial reliability analysis of explosive blast load damage to reinforced concrete columns. Struct. Saf. 53, 13–25.
Sjölander, A., 2017. Analyses of Shotcrete Stress States Due to Varying Lining Thickness and Irregular Rock Surfaces. Licentiate thesis, TRITA–BKN 150. KTH Royal Institute of Technology, Stockholm.
Sjölander, A., Bjureland, W., Ansell, A., 2017. On Failure Probability in Thin Irregular Shotcrete Shells. In ITA-AITES World Tunnel Congress, Bergen Norway, 9–15 June

2017.
Stewart, M.G., Mullard, J.A., 2007. Spatial time-dependent reliability analysis of corrosion damage and the timing of first repair for RC structures. Eng. Struct. 29, 1457–1464.
Timoshenko, S.P., Woinowsky-Krieger, S., 1959. Theory of Plates and Shells. McGraw-hill, New York.
Vanmarcke, E., 1977. Probabilistic modeling of soil profiles. J. Geotech. Eng. Div.-ASCE 103, 1227–1246.
Ventsel, E., Krauthammer, T., 2001. Thin Plates and Shells. Marcel Dekker, New York.